

# Electron Capture by Proton Beam in Collisions with Water Vapor

Sanjeev Kumar Maurya <sup>1</sup>, Abhijeet Bhogale <sup>1,2</sup> and Lokesh C. Tribedi <sup>1,\*</sup>

<sup>1</sup> Department of Nuclear and Atomic Physics, Tata Institute of Fundamental Research, Homi Bhabha Road, Colaba, Mumbai 400005, India

<sup>2</sup> Department of Applied Science, Sardar Patel Institute of Technology, Andheri West, Mumbai 400058, India

\* Correspondence: lokesh@tifr.res.in

**Abstract:** In low energy ion-molecule collisions, electron capture is one of the most important channels. A new experimental setup was developed to study the electron capture process using low-energy ion beams extracted from an electron cyclotron resonance (ECR) plasma-based ion accelerator. Experiments were carried out with the proton beam colliding with water vapor in the energy range of 70–300 keV. Capture events were detected using a position-sensitive detection system comprising micro channel plates (MCPs) and a delay line detector (DLD). These e-capture events can be a result of pure capture reactions as well as transfer ionization. The capture cross section was found to decrease sharply with the beam energy and agreed well with previous measurements. The setup was also used to detect the events that gave rise to the single and multiple e-capture (integrated over all recoil-ion charge states) of C<sup>4+</sup> ions. The capture cross-sections for one, two, three, and four electrons were measured for 100 keV C<sup>4+</sup> ions. The ratio of multielectron capture yield to that for single e-capture decreased with the number of captured electrons.

**Keywords:** ion-molecule collisions; electron capture; water vapor; ECR-ion source; proton



**Citation:** Maurya, S.K.; Bhogale, A.; Tribedi, L.C. Electron Capture by Proton Beam in Collisions with Water Vapor. *Atoms* **2023**, *11*, 21. <https://doi.org/10.3390/atoms11020021>

Academic Editors: Izumi Murakami, Daiji Kato, Hiroyuki A. Sakaue and Hajime Tanuma

Received: 31 October 2022

Revised: 16 January 2023

Accepted: 24 January 2023

Published: 27 January 2023



**Copyright:** © 2023 by the authors. Licensee MDPI, Basel, Switzerland. This article is an open access article distributed under the terms and conditions of the Creative Commons Attribution (CC BY) license (<https://creativecommons.org/licenses/by/4.0/>).

## 1. Introduction

The collision dynamics of multiply charged ions with various molecules is of great importance in many areas such as radiobiology, plasma physics, laser physics, and astrophysics [1–5], in addition to basic atomic molecular physics. Electron capture and ionization are important processes that lead to energy loss for ions penetrating living matter. Theoretical research on these reactions is focused on biological targets such as water and DNA components by using different perturbative quantum-mechanical calculations [6–8]. Water is very important for modelling radiation damage, since about 60–70% of the human body is made up of water. The study of collisions involving heavy ions and water molecules has attracted special attention in recent years due to its application in radiobiology, particularly for radiation therapy or hadron therapy in the treatment of tumors [9–11]. This motivation has made water a benchmark molecule for understanding the collision dynamics of heavy ions colliding with multielectron molecular systems. The perturbative method based on the continuum distorted wave–Eikonal initial state (CDW-EIS) [6] was employed to investigate the ionization of water in collisions with HCl, such as, C<sup>4+</sup>, C<sup>6+</sup>, and Si<sup>13+</sup>, for which experimental results are also available [12–14]. There are also reviews related to the application of heavy-ion beams in tumor therapy [11,15]. Despite the broad range of interest, capture cross-sections involving HCl collisions with water molecules are scarce. Toburen et al. [16] reported the first e-capture cross-sections for proton collisions with H<sub>2</sub>O in the energy range 100–2500 keV, followed by Rudd et al., where the cross-sections were measured in the energy range of 7–4000 keV [17].

In the present work, an experimental setup is described, which was recently developed to study e-capture from atoms and molecules using HCl as projectiles. Initially, the measurements are carried out using a proton beam as projectile and water vapor as a target to validate the experimental setup. Single-capture events were measured and compared

with those from Toburen et al. [16]. We were interested in studying single- and multiple-capture events for  $C^{4+}$  projectiles on water for different energies. The system is capable of providing multiple capture cross-sections in collisions of low energy, highly charged ions, which is not explored much. In the present case, we demonstrated a multiple capture spectrum for a single energy only; that is, for 100 keV  $C^{4+}$  projectiles.

## 2. Experimental Details

Electron cyclotron resonance (ECR) plasmas are used as an ion source in many research areas, such as focused ion beams [18–22], broad ion beams [23], ion accelerators [24], etc., because of their several advantages such as (i) capability to provide variable ion species, (ii) stability of source, (iii) large beam current, (iv) extraction of beam from unmagnetized central dense plasma region, (v) mono-energetic beam with small ion energy spread, and (vi) long lifetime requiring relatively less maintenance [18]. Here, the ECR ion accelerator (ECRIA) on a 400 kV deck [24] was used to extract a low-energy proton beam. The major components of the experimental setup were a gas cell chamber and a position-sensitive detection system comprising two micro channel plates (MCPs) in chevron configuration and a quadrant delay line detector (DLD). For a detailed and clear explanation of the experimental setup and detection of electron capture events, a highly charged ion ( $C^{4+}$ ) beam was considered as the projectile beam as shown in Figure 1.

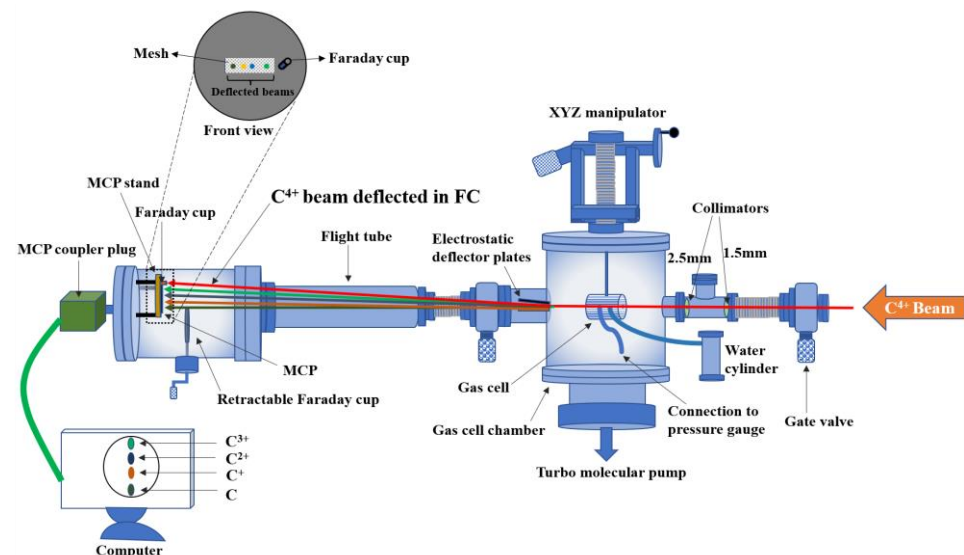


**Figure 1.** Schematic diagram of electron capture experimental setup. MCP: micro channel plate; FC: Faraday cup.

The beam was extracted from the ECR ion source-based low energy accelerator (ECRIA) using 30 kV extraction voltage and two lenses, which consisted of a plasma lens and an Einzel lens. The beam current was maximized by varying the Einzel lens to 0–3.5 kV. The charge state of the ions was selected using a  $90^\circ$ -bending analyzing magnet. An accelerating column was used to accelerate the beam to high energy up to 400 keV/q. The incoming beam was focused, and the beam current was maximized at the Faraday cup (FC-02) using an electrostatic quadrupole lens ( $Q_1$ ) and two sets of electrostatic x–y steerers. The beam was again guided through the beamline to Faraday cup FC-03 and the beam current was maximized using another set of electrostatic quadrupole lenses ( $Q_2$ ) and a set of steerers. The beam was collimated by a set of circular collimators of diameters 1.5 mm and 2.5 mm, which were attached before the experimental chamber. The beam current was optimized by cutting the beam using two 4-jaw slits preceding the circular collimators. Finally, the  $C^{4+}$  beam was passed through the gas cell, and it could capture one to four electrons from water molecules. The position of the gas cell was aligned with the beamline using an XYZ manipulator. The gas cell is comprised of two concentric hollow cylinders of

diameter 2 cm and 5 cm. The length of the inner and outer cylinders were 5 cm and 10 cm, respectively. Both cylinders had apertures of 3 mm at the front and back surfaces, which allowed the beam to pass through. The target gas was put in the inner cylinder. A provision was kept for pumping the outer cylinder, if required for certain collision systems. However, it was not needed in the present experiment. The chamber vacuum was maintained at  $\sim 1 \times 10^{-7}$  mbar or less by using single turbo pump (pumping speed  $\sim 620$  L/s) connected to the main chamber (diameter  $\sim 20$  cm and height  $\sim 25$  cm). The gas flowed directly to the inner cylinder and diffuses to the outer cylinder through an aperture (diameter  $\sim 3$  mm). Therefore, the molecules were randomly oriented unlike a jet, and they dispersed abruptly just outside the inner cell. Therefore, the effective length of the gas cell was taken as 5 cm, i.e., the length of the inner cylinder. To discriminate between single and multiple capture events, electrostatic deflection plates (trapezoidal geometry) were used after the gas cell, which separated the initial beam into  $C^{3+}$ ,  $C^{2+}$ ,  $C^+$ , and neutral C due to capture. The main beam  $C^{4+}$  (or proton) was collected in the Faraday cup of diameter 10 mm and length of 5 cm as shown in Figure 1, while the captured particles were collected on the MCP detector. The Faraday cup had a length-to-diameter ratio  $\sim 5$ . Because of the narrow width and large depth of the Faraday cup, the effect of secondary electron emission was found to be negligible. Most of the low energy electrons which were backscattered were contained in the FC-tube itself and were not lost. Therefore, the correction for secondary electron emission was not included in the beam current measurement. This may have added a small systematic error. A mesh of transmission of 90% was used before the MCP to avoid any fringing field. Here, the fringing field effect implies the influence of the electric field due to the MCP front high voltage on the trajectory of the ion-beams. The main beam current was minimized to  $\sim 200$  fA to optimize the count rate of  $\sim 3$ – $10$  kHz. The beam current was measured using a femtometer controlled by a personal computer (PC) via LabVIEW interfacing. The capture events were detected by the position-sensitive detector. The MCPs had an active diameter of 40 mm and thickness of 1 mm. The pore size in the MCP was  $13 \mu\text{m}$ . The applied voltages to the MCP front and signal were  $-1600$  V and  $360$  V, respectively. The data were collected using Cobold PC software [25]. Figure 2 shows the capture spectrum for the  $C^{4+}$  beam, and the capture channels are well separated.

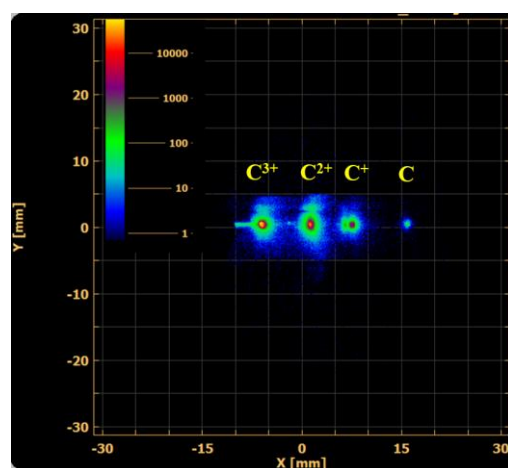


**Figure 2.** Image of the electron capture channels on position sensitive detector (PSD) representing 1-, 2-, 3-, and 4-capture.

For the proton beam, only the single electron capture was investigated. The base pressure in the chamber and the beamline was  $\sim 8 \times 10^{-9}$  mbar. The energy was varied in the range of 70–300 keV and the gas cell pressure was maintained at  $1 \times 10^{-4}$  mbar. The single collision regime was assured at this pressure (mean free path  $\sim 1.15$  m). The beam line vacuum and chamber pressure were increased to  $\sim 1 \times 10^{-8}$  mbar and  $\sim 1 \times 10^{-7}$  mbar, respectively, during the experiment.

### 3. Results and Discussion

The electron capture cross section ( $\sigma_i$ ) is calculated by using the formulae provided below:

$$\sigma_i = \frac{N_{cap} \times q \times 1.6 \times 10^{-19}}{I \times t \times N_t \times l \times OAR \times m} \quad (1)$$

which is used under a thin target or single collision condition. The experiment was performed at a sufficiently low target density. The gas cell pressure was maintained at  $1 \times 10^{-4}$  mbar (mean free path  $\sim 1.15$  m) and the single collision regime was assured at this pressure. The thin target condition was verified by performing the experiment at different water vapor pressures, and the variation of counts in the capture channel (single e-capture) with pressure was studied. A linear behavior of counts with the pressure verified the thin target or single collision conditions. This technique is quite well established. Here,  $\sigma_i$  is the cross section for  $i^{\text{th}}$  e-capture in Figure 2. The  $N_{cap}$  is the number of projectiles on MCP in the  $i^{\text{th}}$  e-capture,  $q$  is the charge state of the projectile, and  $I$  is the beam current at the target. The quantities  $t$ ,  $l$ ,  $OAR$ , and  $m$  are the time of data acquisition, interaction length, open area ratio, and mesh transmission, respectively. The values of other parameters  $l$ ,  $OAR$ , and  $m$  are taken as 5 cm, 60% [25,26], and 90%, respectively, in the calculation. The intrinsic efficiency is included in the  $OAR$  parameter [26]. Here,  $N_t$  is the number density of the target in a static gas pressure condition, which is calculated by

$$N_t = 9.659 \times 10^{15} \frac{P(mTorr)}{T(K)} \quad (2)$$

where  $P$  and  $T$  are the neutral gas pressure in the gas cell and temperature of the gas, which is taken as room temperature.

A single peak corresponding to a single electron capture by proton beam in collisions with water vapor is shown in Figure 3a. The counts in Figure 3a are normalized with respect to the main beam. The measured cross section  $\sigma_1$  for single capture by proton is shown in Figure 3b. The capture cross-section was found to decrease sharply with projectile energy. The data of Toburen et al. [16] show an excellent agreement with the present experiment. The present data and Toburen et al.'s data are tabulated in Table 1.

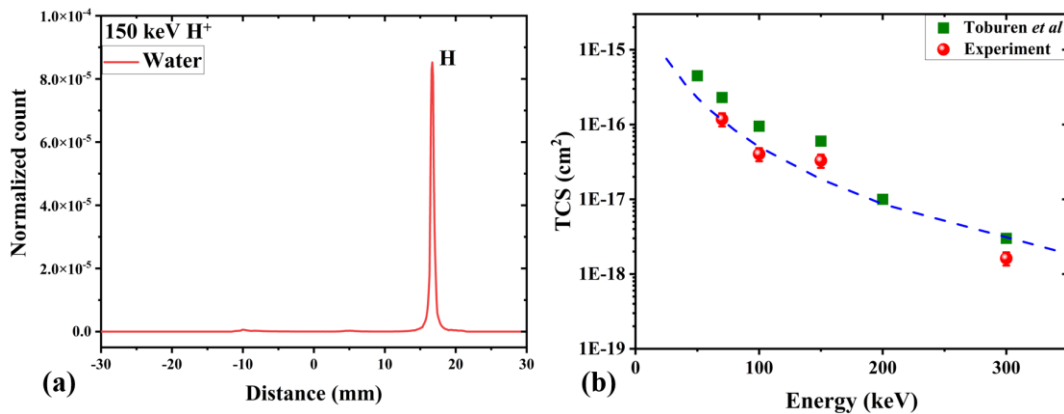


**Figure 3.** (a) Normalized counts for 150 keV  $\text{H}^+$  collisions with water. (b) Single e-capture cross section in collisions of  $\text{H}^+$  with water at different beam energies (red circle: present data; green square: Toburen et al. [16]). Dashed lines are guides for the eye.

**Table 1.** The present total cross-section (TCS) data with Toburen et al. [16]. Numerals in brackets indicate the power of 10. The experimental error in the present data is ~20%.

Energy (keV)	TCS (cm <sup>2</sup> )	
	Present	Toburen et al.
70	2.4 (−16)	2.3 (−16)
100	8.1 (−17)	9.5 (−17)
150	6.6 (−17)	6.0 (−17)
300	3.2 (−18)	3.0 (−18)

The setup is capable of detecting multiple e-capture events. This is displayed in Figure 2 for 100 keV C<sup>4+</sup> projectiles and single and multiple capture channels. Figure 4a shows the counts for different capture channels and the same data are shown in a linear scale in Figure 4b. Here, the counts in Figure 4a,b are normalized with respect to the main beam. One can clearly see the peaks corresponding to one, two, three, and four e-capture events. It is observed that only the peak of neutral C is largely separated from other peaks as this is the neutral beam and follows the beamline direction. The difference in the distance between the other peaks (C<sup>+</sup>, C<sup>2+</sup>, and C<sup>3+</sup>) is very small. The distance between the peaks of C<sup>+</sup> and C<sup>2+</sup> is ~6.7 mm and for C<sup>2+</sup> and C<sup>3+</sup>, it is observed to be ~7.7 mm. Therefore, a small difference of 1 mm is seen between the peaks of C<sup>+</sup>, C<sup>2+</sup>, and C<sup>3+</sup>. A SIMION simulation was carried out to understand this part. The SIMION beam simulation showed no difference in the peak position when the beam was assumed at the center of the beam line. However, a difference of 0.5 mm was observed when the input beam was taken at 1 mm above the center. Moreover, the beam diameter coming out of the gas cell was slightly wider due to the intrinsic divergence of the ECR ion beams. The gas cell inlet and outlet were of 3 mm diameter. Therefore, considering the width of the beam and the possible shift of the incident ions, it could cause a nonuniform separation of about 1 mm.

The cross-section for each capture channel (Figure 4c) was found to decrease with the number of captured electrons. The ratio of multi e-capture to single capture cross sections, i.e.,  $\sigma_2/\sigma_1, \sigma_3/\sigma_1, \sigma_4/\sigma_1$ , are also plotted in Figure 4d. The ratios were found to decrease with the number of e-captured channels,  $\sigma_2/\sigma_1 \sim 0.377, \sigma_3/\sigma_1 \sim 0.105$ , and  $\sigma_4/\sigma_1 \sim 0.004$ . The measured cross-section and the calculated ratio of multi to single e-captures are tabulated in Table 2.

**Table 2.** The measured cross-section and the calculated ratio of multi to single e-capture for 100 keV C<sup>4+</sup> projectiles. Numerals in square brackets indicate the power of 10. The experimental error in the cross section is ~20%.

Number of Captured Electrons	Cross-Section (10 <sup>−16</sup> cm <sup>2</sup> )	Ratio of Multi E-Capture to Single Capture
1	13.1	1.000
2	12.0	0.377
3	3.41	0.105
4	0.132	0.004

Note that the capture events could be produced in such a way that the target could be ionized apart from the electron capture. Since no coincidence with recoil ions was taken, the present data are the sum of pure capture and transfer-ionization. In the case of C<sup>4+</sup> projectiles, the transfer-ionization series are important. However, for protons, these processes are qualitatively much smaller [27]. The present system measures the cross sections for single and multiple electron capture channels using a gas cell, deflector plates, and position-sensitive detector assembly. These are, however, total capture, since these include the transfer ionization contributions too and these are data useful for the simulation of energy loss at the Bragg peak of hadron therapy, which traditionally uses C<sup>4+</sup> ions—which could be of important significance. The present system can be combined with a

time-of-flight recoil ion momentum spectrometer system to measure the cross sections for pure capture and transfer ionization separately for various highly charged ions for water as well as for other biomolecules/PAH molecules.

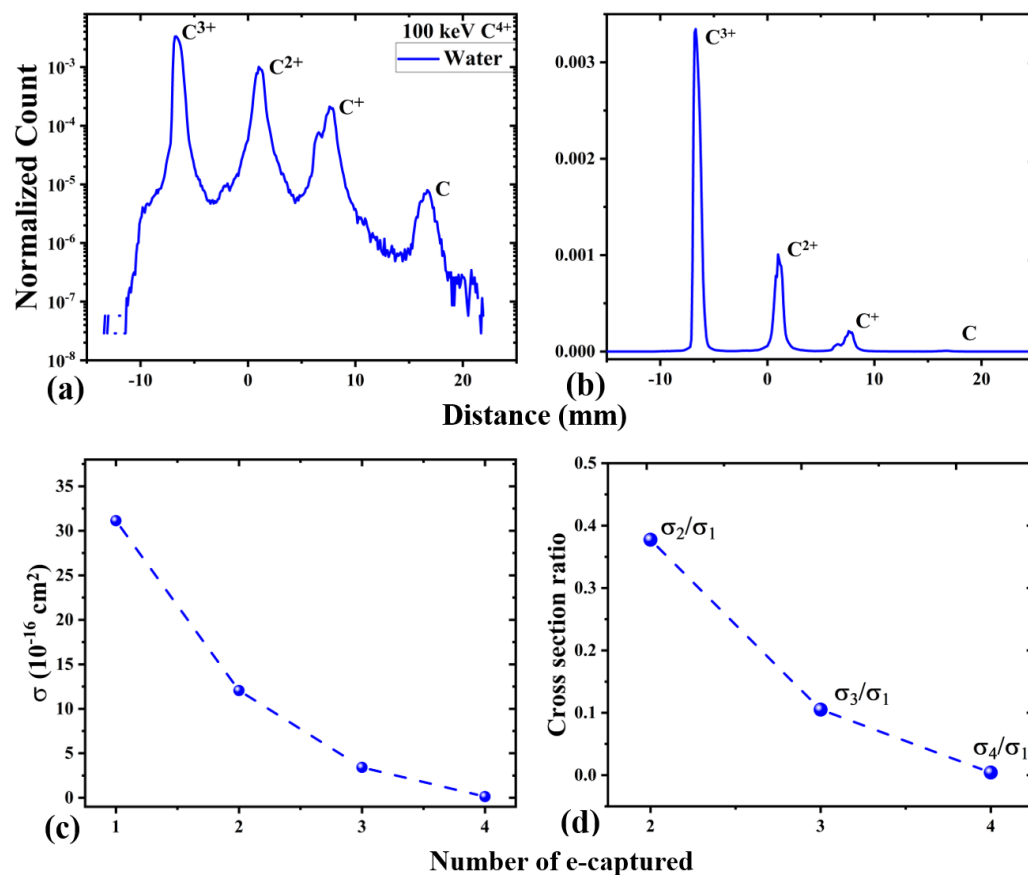


**Figure 4.** (a) Normalized counts with distance on position sensitive detector, for 100 keV  $C^{4+}$  collisions with water, showing distinct peaks of  $C$ ,  $C^+$ ,  $C^{2+}$ , and  $C^{3+}$  capture channels. (b) The same data are shown in a linear scale. (c) Cross-section for different electron capture channels with number of captured electrons. (d) The ratio of multi-capture to single capture cross-section for 100 keV  $C^{4+}$  beam. Dashed lines are guides to the eye.

#### 4. Conclusions

A new experimental setup was developed to measure the electron capture cross-sections for single and multiple capture channels using a gas cell, deflector plates, and position-sensitive detector assembly. The single electron capture cross-section was measured in collisions of the proton beam with water vapor. The single e-capture cross-sections decreased sharply with proton beam energy. The experimental results were compared with earlier-reported capture cross-sections and excellent agreement was found. We applied the experimental system for  $C^{4+}$  projectiles and the 2-, 3-, and 4-capture events were clearly detected for the water target. The capture cross-section was measured for each capture channel for 100 keV  $C^{4+}$  ions. The ratios of multi-capture relative to single electron capture channels were found to be ~38%, 11%, and 0.4%, respectively, for 100 keV  $C^{4+}$  projectile energy. In this case, the capture events were integrated over all recoil-ion charge states including single or multiple transfer ionizations.

**Author Contributions:** Conceptualization, L.C.T.; methodology, L.C.T., S.K.M. and A.B.; software, S.K.M., A.B. and L.C.T.; validation, L.C.T. and S.K.M.; formal analysis, S.K.M. and A.B.; investigation, A.B., S.K.M. and L.C.T.; resources, L.C.T.; data curation, S.K.M., A.B.; writing—original draft preparation, L.C.T. and S.K.M.; writing—review and editing, L.C.T. and S.K.M.; visualization, S.K.M. and L.C.T.; supervision, L.C.T.; project administration, L.C.T.; funding acquisition, L.C.T. All authors have read and agreed to the published version of the manuscript.

**Funding:** This research was funded by DEPARTMENT OF ATOMIC ENERGY, GOVERNMENT OF INDIA, project No. 12P-R\D-TFR-5.02-0300.

**Data Availability Statement:** No further research-data is available publicly at the moment.

**Acknowledgments:** We acknowledge the Central Workshop, TIFR, Mumbai, for the timely fabrication of components. We would like to thank the scientific staff (Nilesh Mhatre, K.V.T. Ram, D. Pathare, and S. Manjrekar) at TIFR for the smooth operation of the machine and other technical support. Authors also thank Chandan Bagdia for his help and discussions.

**Conflicts of Interest:** The authors declare no conflict of interest.

## References

1. McDaniel, E.W.; Mitchell, J.B.A.; Rudd, M.E. *Atomic Collisions*; Wiley: New York, NY, USA, 1993.
2. Enos, C.S.; Lee, A.R.; Brenton, A.G. Electronic excitation of atmospheric molecules by proton impact. *Int. J. Mass Spectrom. Ion Process* **1991**, *104*, 137. [[CrossRef](#)]
3. Townsend, L.W.; Wilson, J.W.; Cucinotta, F.A.; Shinn, J.L. Galactic Cosmic Ray Transport Methods and Radiation Quality Issues. *Int. J. Radiat. Appl. Instrum Part D Nucl. Tracks Radiat. Meas.* **1992**, *20*, 65–72. [[CrossRef](#)] [[PubMed](#)]
4. Amaldi, U.; Kraft, G. Radiotherapy with Beams of Carbon Ions. *Rep. Prog. Phys.* **2005**, *68*, 1861–1882. [[CrossRef](#)]
5. Inokuti, M. Inelastic Collisions of Fast Charged Particles with Atoms and Molecules- The Bethe Theory Revisited. *Rev. Mod. Phys.* **1971**, *43*, 297–347. [[CrossRef](#)]
6. Champion, C.; Weck, P.F.; Lekadir, H.; Galassi, M.E.; Fojón, O.A.; Abufager, P.; Rivarola, R.D.; Hanssen, J. Proton-induced single electron capture on DNA/RNA bases. *Phys. Med. Biol.* **2012**, *57*, 3039. [[CrossRef](#)] [[PubMed](#)]
7. Tachino, C.A.; Monti, J.M.; Fojón, O.A.; Champion, C.; Rivarola, R.D. Ionization of water molecules by ion beams. On the relevance of dynamic screening and the influence of the description of the initial state. *J. Phys. B At. Mol. Opt. Phys.* **2014**, *47*, 035203. [[CrossRef](#)]
8. Mendez, A.M.P.; Montanari, C.C.; Miraglia, J.E. Ionization of biological molecules by multicharged ions using the stoichiometric model. *J. Phys. B At. Mol. Opt. Phys.* **2020**, *53*, 055201, Correction: *J. Phys. B At. Mol. Opt. Phys.* **2020**, *53*, 249501. [[CrossRef](#)]
9. Levin, W.P.; Kooy, H.; Loeffler, J.S.; DeLaney, T.F. Proton beam therapy. *Brit. J. Cancer* **2005**, *93*, 849. [[CrossRef](#)] [[PubMed](#)]
10. Smith, A.R. Proton therapy. *Phys. Med. Biol.* **2006**, *51*, R491. [[CrossRef](#)] [[PubMed](#)]
11. Scharadt, D.; Elsasser, T.; Schulz-Ertner, D. Heavy-ion tumor therapy: Physical and radiobiological benefits. *Rev. Mod. Phys.* **2010**, *82*, 383–425. [[CrossRef](#)]
12. Ohsawa, D.; Tawara, H.; Soga, F.; Galassi, M.E.; Rivarola, R.D. 6.0 MeV u<sup>-1</sup> carbon ion (C<sup>6+</sup> and C<sup>4+</sup>)-induced secondary electron emission from water vapor. *Phys. Scr.* **2013**, *T156*, 014039. [[CrossRef](#)]
13. Bhattacharjee, S.; Biswas, S.; Monti, J.M.; Rivarola, R.D.; Tribedi, L.C. Double-differential cross section for ionization of H<sub>2</sub>O molecules by 4-MeV/u C<sup>6+</sup> and Si<sup>13+</sup> ions. *Phys. Rev. A* **2017**, *96*, 052707. [[CrossRef](#)]
14. Luna, H.; Wolff, W.; Montenegro, E.C.; Tavares, A.C.; Ludde, H.J.; Schenk, G.; Horbatsch, M.; Kirchner, T. Ionization and electron-capture cross sections for single- and multiple-electron removal from H<sub>2</sub>O by Li<sup>3+</sup> impact. *Phys. Rev. A* **2016**, *93*, 052705. [[CrossRef](#)]
15. Nikjoo, H.; Emfietzoglou, D.; Liamsuwan, T.; Taleei, R.; Liljequist, D.; Uehara, S. Radiation track, DNA damage and response—A review. *Rep. Prog. Phys.* **2016**, *79*, 116601. [[CrossRef](#)]
16. Toburen, L.H.; Nakai, M.Y.; Langley, R.A. Measurement of High-Energy Charge-Transfer Cross Sections for Incident Protons and Atomic Hydrogen in Various Gases\*. *Phys. Rev.* **1968**, *171*, 114. [[CrossRef](#)]
17. Rudd, M.E.; Goffe, T.V.; DuBois, R.D.; Toburen, L.H. Cross sections for ionization of water vapor by 7-4000-keV protons. *Phys. Rev. A* **1985**, *31*, 492. [[CrossRef](#)] [[PubMed](#)]
18. Maurya, S.K.; Bhattacharjee, S. Variable gaseous ion beams from plasmas driven by electromagnetic waves for nano-micro structuring: A tutorial and an overview of recent works and future prospects. *Plasma Res. Express* **2020**, *2*, 033001. [[CrossRef](#)]
19. Maurya, S.K.; Paul, S.; Shah, J.K.; Chatterjee, S.; Bhattacharjee, S. Momentum transfer using variable gaseous plasma ion beams and creation of high aspect ratio microstructures. *J. Appl. Phys.* **2017**, *121*, 123302. [[CrossRef](#)]
20. Maurya, S.K.; Barman, S.; Pan, N.; Bhattacharjee, S. Effect of plasma and beam parameters on focal dimensions in micrometer charged particle optics: Enhanced nonlinear demagnification below the Debye length. *Phys. Plasmas* **2019**, *26*, 063103. [[CrossRef](#)]
21. Maurya, S.K.; Barman, S.; Bhattacharjee, S. Charge dissipation and self focusing limit in high current density ion beam transport through a micro glass capillary. *J. Phys. D Appl. Phys.* **2019**, *52*, 055205. [[CrossRef](#)]

22. Barman, S.; Maurya, S.K.; Bhattacharjee, S. Experimental realization of nonlinear demagnification in plasma-based charged particle optics. *Plasma Res. Express* **2022**, *4*, 025003. [[CrossRef](#)]
23. Chatterjee, S.; Bhattacharjee, S.; Maurya, S.K.; Srinivasan, V.; Khare, K.; Khandekar, S. Surface wettability of an atomically heterogeneous system and the resulting intermolecular forces. *Euro Phys. Lett.* **2017**, *118*, 68006. [[CrossRef](#)]
24. Agnihotri, A.N.; Kelkar, A.H.; Kasthurirangan, S.; Thulasiram, K.V.; Desai, C.A.; Fernandez, W.A.; Tribedi, L.C. An ECR ion source-based low-energy ion accelerator: Development and performance. *Phys. Scr.* **2011**, *T144*, 014038. [[CrossRef](#)]
25. Available online: <https://www.roentdek.com> (accessed on 10 January 2023).
26. Krems, M.; Zirbel, J.; Thomason, M.; DuBoisa, R.D. Channel electron multiplier and channelplate efficiencies for detecting positive ions. *Rev. Sci. Instrum.* **2005**, *76*, 093305. [[CrossRef](#)]
27. Dunseath, K.M.; Crothers, D.S.F. Transfer and ionization processes during the collision of fast  $H^+$ ,  $He^{2+}$  nuclei with helium. *J. Phys. B At. Mol. Opt. Phys.* **1991**, *24*, 5003–5022. [[CrossRef](#)]

**Disclaimer/Publisher’s Note:** The statements, opinions and data contained in all publications are solely those of the individual author(s) and contributor(s) and not of MDPI and/or the editor(s). MDPI and/or the editor(s) disclaim responsibility for any injury to people or property resulting from any ideas, methods, instructions or products referred to in the content.